ACS APPLIED MATERIALS & INTERFACES

Research Article

www.acsami.org

Fabrication of LiF/Fe/Graphene Nanocomposites As Cathode Material for Lithium-Ion Batteries

Ruguang Ma,[†] Yucheng Dong,[†] Liujiang Xi,[†] Shiliu Yang,[†] Zhouguang Lu,*[,‡] and Chiyuen Chung*[,†]

[†]Department of Physics and Materials Science, City University of Hong Kong, 83 Tat Chee Avenue, Kowloon, Hong Kong, China

[‡]Department of Micro & Nano Materials and Devices, South University of Science and Technology of China, Shenzhen, Guangdong, China

Supporting Information

ABSTRACT: Homogeneous LiF/Fe/Graphene nanocomposites as cathode material for lithium ion batteries have been synthesized for the first time by a facile two-step strategy, which not only avoids the use of highly corrosive reagents and expensive precursors but also fully takes advantage of the excellent electronic conductivity of graphene. The capacity remains higher than 150 mA h g^{-1} after 180 cylces, indicating high reversible capacity and stable cyclability. The ex situ XRD and HRTEM investigations on the cycled LiF/Fe/G nanocomposites confirm the formation of FeF_x and the coexistence of LiF and FeF_x at the charged state. Therefore, the heterostructure nanocomposites of LiF/Fe/Graphene with nano-LiF and ultrafine Fe homogeneously anchored on graphene sheets could open up a novel avenue for the application of iron fluorides as high-performance cathode materials for lithium-ion batteries.

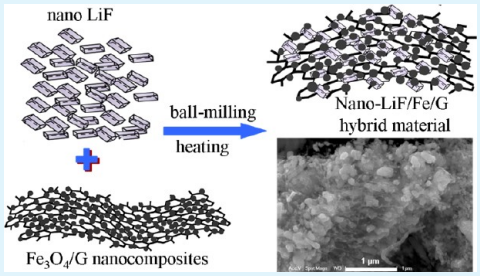

KEYWORDS: *fluorides, graphene, nanocomposites, ball-milling, conversion reaction, lithium ion batteries*

1. INTRODUCTION

Nowadays, lithium ion batteries (LIBs) as power sources have dominated the market of portable electronic devices,[1−3] but its commercial application in large-scale energy storage systems, such as electric vehicles and power backups, remains to be a fascinating challenge. The nature of only transferring 0.5−1.0 electrons per formula unit during charge/discharge, limits the specific capaicty of the conventional intercalation compounds like $LiCoO_2$, $LiMn_2O_4$, $LiFePO_4$, etc., largely restricting their wide application. Therefore ever-increasing effort has been dedicated to developing advanced materials with high energy and power density.[4−8] Transition metal (TM) fluorides based on conversion reaction have attracted considerable interest.[9−12] During the electrochemical charge/discharge, more than one electron per formula unit takes part in the redox reaction as shown in eq 1, which results in improved specific storage capacity.

$$TM^{n+}F_n + ne^- + nLi^+ \leftrightarrow TM + nLiF \quad (1)$$

Among the TM fluorides, iron fluorides (FeF_x) are the most promising electrode material, due to their many superior properties, such as high theoretical specific capacity (712 for FeF_3 and 571 mA h g^{-1} for FeF_2), low cost and good thermal stability.[5,13]

However, the application of FeF_x as a cathode material for LIBs has been largely hindered by its low electronic conductivity. Making TM fluoride-carbon nanocomposites[14−17] is one of the most feasible strategies to enhance the electronic condcutivity. For example, FeF_3 nanoflowers have been directly grown on carbon nanotubes, demonstrating a reversible capacity of 200 mA h g^{-1} at a current density of 20 mA g^{-1} between 2.0 and 4.5 V.[15] Iron fluoride nanoparticles cross-linked by single-wall carbon nanotube (SWNT) have also been synthesized by utilizing ionic liquid.[16] A composite of SWNT-$FeF_3{\cdot}0.33H_2O$ delivered a specific capacity of about 220 mA h g^{-1} in the initial cycle and 145 mA h g^{-1} after 50 cycles at a current density of 23.7 mA g^{-1} in the voltage range of 1.7−4.5 V. Wang's group also prepared MoS_2/FeF_3 and V_2O_5/FeF_3 by ball-milling to improve the conductivity of FeF_3, demostrating enhanced electrochemical performance.[18,19]

On the other hand, seeking solutions from the right side of eqution 1, synthesizing carbon-TM-LiF nanocomposites,[20−23] was also seriously considered. Li et al studied the electrochemical activity of LiF in the form of TM/LiF and revealed the general possibility of a reversible formation and decomposition of LiF.[20] Doe et al investigated the Li−Fe−F phase diagram and conversion reaction of iron fluorides with Li by employing the first principles method and explained why a rutile FeF_2-like structure can form upon charging the mixture of LiF and Fe with a molar ratio of 3:1.[12] Prakash et al., successfully obtained C/Fe/LiF nanocomposites with stable and high capacity by pyrolyzing the starting materials of ferrocene and LiF at an elevated temperature.[24,25] The nanocomposite delivered a stable capacity of 275 mA h g^{-1} in the potential range between 4.3 and 0.5 V at 20.83 mA g^{-1}

Received: November 3, 2012
Accepted: January 8, 2013
Published: January 8, 2013

and capacity remained 170 mA h g^{-1} after 30 cycles between 4.3 and 1.3 V.

Graphene has attracted great recent interest owing to its excellent electronic conductivity, superior mechanical flexibility and high theoretical surface area.[26,27] For LIBs, graphene has been used to form nanocomposites with SnO_2,[28] TiO_2,[29] Fe_3O_4,[30,31] Co_3O_4,[32] and MnO[33] in an attempt to improve the electronic conductivity and cycling stability of the electrode materials. Based on the fabrication of metal oxide/graphene nanocomposites, herein, we proposed a two-step method to synthesize uniform LiF/Fe/Graphene nanocomposites (nano-LiF/Fe/G) as cathode material for LIBs. Two prominent advantages of this method are (1) skillfully avoiding highly erosive reagents (e.g., HF) and expensive precursors (e.g., ionic liquid) during the fabrication process and (2) sufficiently taking advantage of the excellent electronic conductivity of graphene during charge/discharge process. Moreover, this technique is easy for scale-up productions.

2. EXPERIMENTAL SECTION

Fabrication of Fe_3O_4/G. The Fe_3O_4/G nanocomposite was prepared by a simple hydrothermal evaporation-induced method. In a typical synthesis, 40 mg of GO was dispersed in 20 mL of N, N-Dimethylformamide (DMF; anhydrous, 99.8%, Sigma-Aldrich) by mild sonication in an ultrasound bath for 15 min to form a clear, light yellow solution. Then, 1.059 mg of Iron(III) acetylacetonate ($Fe(acac)_3$, 97%, Aldrich) was added into the resulting solution and stirred at 80 °C for 1 h. The resulting solution was transferred to a glass bottle (30 mL in volume), which was then heated from room temperature to 180 °C at a heating rate of 2.5 °C min^{-1} in an electric oven till the DMF solution evaporated completely. After cooling down to room temperature, the product was collected from the bottle. After drying, the powder was heat-treated at 450 °C under 95%Ar/5%H_2 atmosphere to obtain the final Fe_3O_4/G.

Fabrication of Nano-LiF/Fe/G. Nano-LiF was prepared through the wet ball-milling of micro-LiF particles. First, microsize LiF powders were put into a PVDF vial with a certain amount of ethanol, in which the weight ratio of ball (ZrO_2) to powder was 30:1. Then the powder was ball-milled to nanoscale at a speed of 400 rpm for 30 h by using a QM planetary ball mill (Nanjing NanDa Instrument Plant). After that, the powder was dried in a vacuum oven for 10h. To get a uniform and homogeneous mixture, the nano-LiF and Fe_3O_4/G with a molar ratio of 9:1 were mixed by ball-milling at a low speed of 150 rpm for 10h. Nano-LiF/Fe/G hybrid material was obtained by heating the ball-milled nano-LiF/Fe_3O_4/G at 550 °C for 4h under continuous 95%Ar/5%H_2 gas flow. For comparison, micro-LiF/Fe/G was fabricated by the similar procedure except that the nano-LiF was replaced with micro-LiF. And LiF/Fe/Carbon-black nanocomposite was prepared with the same procedure as nano-LiF/Fe/G, except replacing graphene with carbon black.

Characterization. The as-prepared products were characterized using X-ray diffraction (XRD, Philips PW 1830 with Cu Kα radiation) in the 2θ range of 10−90° at a scan rate of 0.02° s^{-1}. To investigate the approximate proportion of carbon in the synthesized products, thermogravimetric analysis (TGA, Q50) was carried out from room temperature to 800 °C under an air ventilation of 10 mL min^{-1} at a heating rate of 20 °C min^{-1}. The morphological characteristics were investigated by scanning electron microscope (SEM, JEOL-820) and transmission electron microscope (TEM; CM200 FEG operated at 200 kV). For examining the morphology of the cycled electrodes, the experimental Li-ion cells were disassembled in an Ar-filled glovebox and rinsed in dimethyl carbonate (DMC) and ethanol for several times.

Electrochemical Measurement. The electrochemical measurements were performed using coin cells (CR-2032) with lithium metal foil (Aldrich, USA) as a counter electrode. The working electrodes were prepared by mixing 80 wt % active material (nano-LiF/Fe/G), 10 wt % acetylene carbon black, and 10 wt % polyvinylidene fluoride (PVDF) binder dissolved in 1-methyl-2-pyrrolidinone (NMP) solvent. The resulting slurry was coated homogeneously on an aluminum foil and dried at 100 °C for 10 h in a vacuum oven and then punched to circular discs (1.6 cm^2) from the Al foil. The punched discs were weighed to determine the amount of active materials before assembled into coin-type cell. One layer of Celgard 2032 (Celgard, Inc., USA) served as the separator and $LiPF_6$ (1 mol/L) was dissolved in a mixture of ethylene carbonate/dimethyl carbonate (1:1 in volume) as the electrolyte. The cells were assembled in a glovebox filled with high purity argon gas with low moisture and oxygen. Galvanostatic discharge/charge cycling measurement of the assembled cells were tested in the voltage range from 1.5 to 4.5 V at a current density of 20.8 mA g^{-1} on an Arbin Instruments (BT 2000, College Station, Texas, USA) battery cycler at room temperature.

3. RESULTS AND DISCUSSION

Figure 1a shows the TEM image of the Fe_3O_4/G nanocomposites. It is clear that Fe_3O_4 nanopatricles with a size of

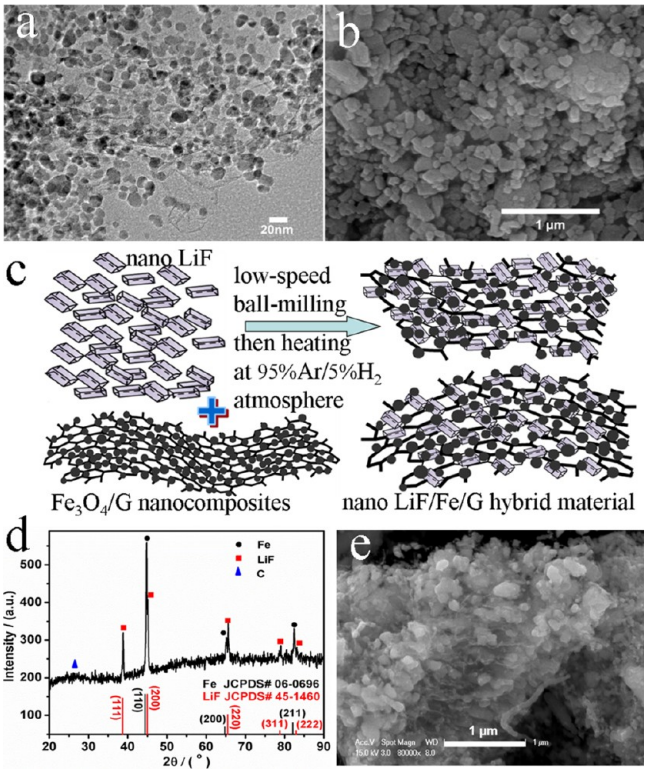

Figure 1. (a) TEM image of Fe_3O_4/G nanocomposites; (b) SEM image of nano-LiF; (c) schematic illustration of fabrication procedure; (d) XRD pattern; and (e) SEM image of the nano-LiF/Fe/G.

10−20 nm are homogeneously anchored on the graphene sheets. Figure S1 in the Supporting Information shows the XRD pattern of the as-synthesized Fe_3O_4/G. The diffractions are in good agreement with those of pure Fe_3O_4 (Magnetite, JCPDS No.85−1436). On the basis of the TGA curve of Fe_3O_4/G under air (see Figure S2a in the Supporting Information) and the XRD of the final residue (see Figure S2b in the Supporting Information), the graphene content was calculated to be about 25.9%. Hence, the weight percentage of Fe_3O_4 was about 74.1% in the Fe_3O_4/G nanocomposities. The weight ratio of Fe to Graphene in the nano-LiF/Fe/G was estimated to be 2:1 by assuming that the Fe_3O_4 in Fe_3O_4/G was completely reduced into Fe. All the following calculations, such

dx.doi.org/10.1021/am302558w | ACS Appl. Mater. Interfaces 2013, 5, 892−897

as the weight percentage of Fe in the active material, were based on this result. After high-speed ball-milling, the cubic micro-LiF (see Figure S3 in the Supporting Information) has converted into fine LiF nanoparticles with an average size of 100 nm (Figure 1b). The synthesis procedure of nano-LiF/Fe/G hybrid material is schematically illustrated in Figure 1c. First, to get a homogeneious mixture, the as-prepared nano-LiF and Fe_3O_4/G in a molar ratio of 9:1 were ball-milled for 10h at a speed of 150 rpm. Then, the ball-milled mixture was calcined at 550 °C for 4h under a continuous 95%Ar/5%H_2 gas flow, faciliating the final reduction of nano-LiF/Fe_3O_4/G to nano-LiF/Fe/G.

XRD pattern in Figure 1d agrees well with α-Fe (JCPDS No.06−0696) and LiF (JCPDS No.45−1460), confirming that nano-LiF/Fe_3O_4/G has completely transformed into nano-LiF/Fe/G after heat-treatment in the 95%Ar/5%H_2 reductive atmosphere. The broad and hump peak appearing at about 26.6° can be ascribed to graphene. SEM image in Figure 1e shows the morphology of the obtained nano-LiF/Fe/G hybrid material, demonstrating that nano-LiF and Fe/G have been homogeneously mixed together. The nanoparticles of Fe and nano-LiF were highly dispersed on graphene sheets or well wrapped by the graphene sheets. This cross-linked characteristics will be beneficial for the prompt transport of electrons, thus improving the electronic conductivity of the electrode.

Figure 2 shows the TEM image of nano-LiF/Fe/G. The inset shows the overview TEM image of the as-prepared nano-LiF/

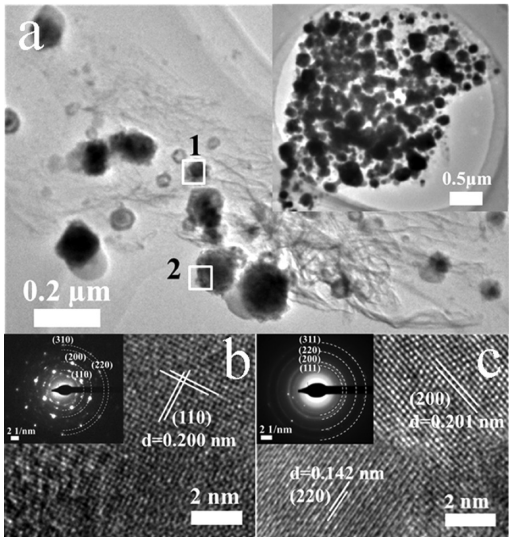

Figure 2. (a) TEM image of the nano-LiF/Fe/G; inset, overview TEM image of nano-LiF/Fe/G; (b, c) HRTEM images of areas as marked by white square "1" and "2" in a, respectively. Insets in b and c are the corresponding SAED images.

Fe/G. It can be seen that there are mainly two kinds of particles, the larger one with size of 100−150 nm and the smaller one with size of 50−60 nm, anchoring on the graphene sheets. Images b and c in Figure 2 show the high-resolution TEM (HRTEM) image of the area as marked by white square "1" and "2" in Figure 2a, respectively. The lattcie spacing in Figure 2b is about 0.200 nm, in agreement with the *d* value of plane (100) of metallic Fe (JCPDS No. 06−0696). The selected area electron diffraction (SAED) dots in the inset of Figure 2b can be indexed to the planes of (110), (200), (220), and (310) corresponding to metallic Fe. It indicates that the small particles are metallic Fe particles that were reduced from Fe_3O_4. The weak diffraction rings demonstrate a polycrystalline and poor crystallinity nature of the Fe nanoparticle. The HRTEM image of the big particle as shown in Figure 2c reveals interplane spacings of 0.201 and 0.143 nm which can be ascribed to the (200) and (220) plane of LiF (JCPDS No.45−1460),respectively. The SAED in inset of Figure 2c can be indexed to planes of (111), (200), (220) and (311) of LiF. Therefore, the large particles with size of 100−150 nm could be ascribed to LiF, whereas the small particles with size of 50−60 nm could be attributed to Fe particles, which are consistent with the observation in images a and b in Figure 1.

To evalutate the electrochemical performance of the hybrid material, we performed galvanostatic charge/discharge experiments at a current density of 20.8 mA g^{-1} in the potential range of 4.5−1.5 V at room temperature. Figure 3a shows the voltage

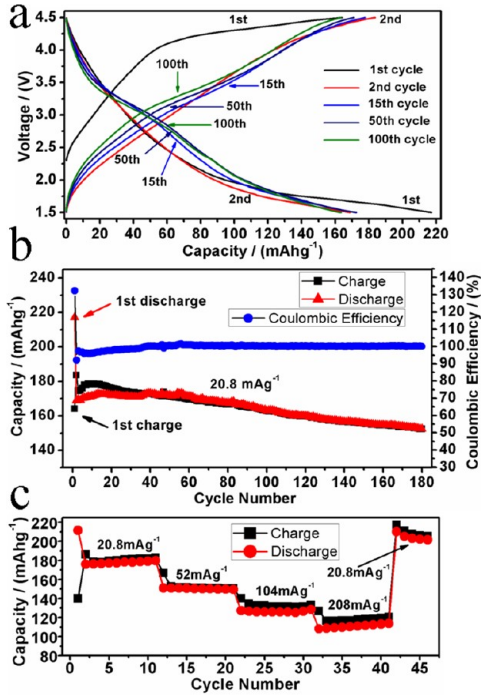

Figure 3. (a) Galvanostatic charge and discharge curves of the nano-LiF/Fe/G in the 1st, 2nd, 15th, 50th, and 100th cycle at 20.8 mA g^{-1} in the potential range of 4.5−1.5 V; (b, c) the cycling performance/Coulombic efficiency and rate capability, respectively.

profiles of the first, second, 15th, 50th, and 100th cycles. The nano-LiF/Fe/G delivered an initial charge and discharge capacity of 164 and 217 mA h g^{-1}, respectively. The initial charge capacity is relatively lower as compared with the literature[10] which can be ascribed to the incomplete delithation of nano-LiF/Fe/G due to the relatively larger particle size of the LiF with a size of about 100 nm. After the activiation of the first cycle, most of the LiF particles were pulverized by discharging, so the charge capacity of the second cycle increased to 184 mA h g^{-1}. We also note that during the first two cycles there is no obvious plateau in the voltage region of 3.5−2.5 V. However, at the 15th cycle, the discharging plateau in this region became clearer, indicating that a further lithiation process arising from the pulverization of active material took place in this voltage range. As the proceeding of cycling, the plateau became more and more obvious, as shown in discharging curves of the 50th and 100th cycles. Meanwhile,

dx.doi.org/10.1021/am302558w | ACS Appl. Mater. Interfaces 2013, 5, 892−897

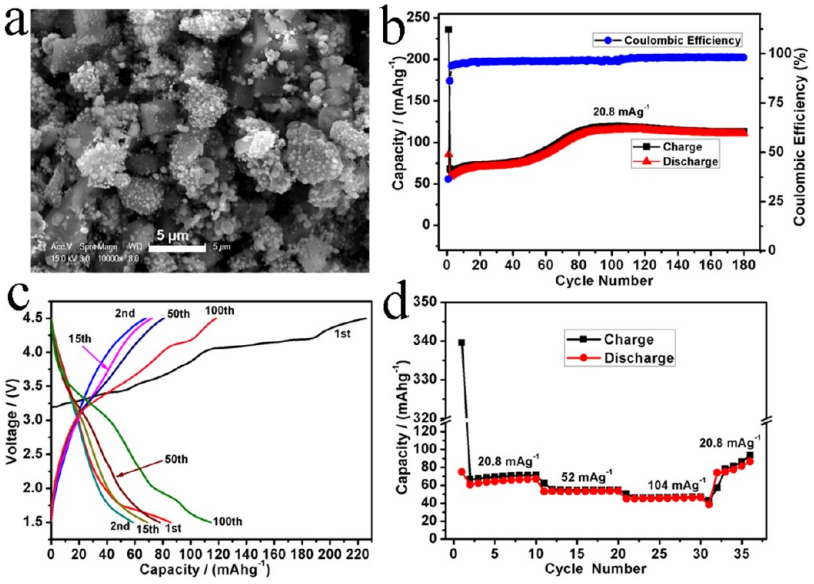

Figure 4. (a) SEM image, (b) cycling performance, (c) voltage profiles, and (d) rate capability of micro-LiF/Fe/G hybrid material.

a tiny plateau in the voltage range of 2.5−2.0 V became apparent, indicating a lithiation process occurred. The evolution of the plateaus is consistent with the variation tendency of charge/discharge capacity and Coulombic efficiency in Figure 3b. It is observed that before the 10th cycle, both the charge and discharge capacities increased silightly with cycle number. And during the first 15 cycles, the Coulombic efficiency was lower than 97%, then increased up to about 100%. This can be attributed to the relatively big particle size of ∼100 nm of the current LiF. After 15 cycles the active material of nano-LiF/Fe/G became very ultrafine and homogeneous, so that both capacity and Coulombic efficency were improved. From the 15th to 60th cycles, the discharge capacity of the hybrid material kept higher than 170 mA h g^{-1} for 45 cycles. The reversible capacity remained to be higher than 150 mA h g^{-1} after 180 cycles, which is better than that reported in the literature.[24] It is speculated that the capaicty can be further improved when the LiF particle size is reduced to tens of nanometers by utilizing high-energy ball-milling.

Figure 3c demonstrates the superior rate capability of the as-obtained nano-LiF/Fe/G. At a low rate of 20.8 mA g^{-1}, the nanocomposite delivered a discharge capacity of ∼175 mA h g^{-1}. As the current density was increased to 52, 104, and 208 mA g^{-1}, the discharge capacity decreased to 149, 126, and 111 mA h g^{-1}, corresponding to a capacity retention of 85.2, 72, 63.5% as reference to the capacity at low rate (20.8 mA g^{-1}), respectively. This rate performance is superior to that reported in ref 25, which can be attributed to the excellent electronic conductivity of the graphene and the very special architecture of close cross-linking of LiF, Fe, and graphene. At relatively high rate (e.g., 104 and 208 mA g^{-1}), the Coulombic efficiency decreased slightly. This could be explained by the concentration polarization of Li^+ in the active material resulting from a diffusion limited process.[34] When the current density was returned to the initial value of 20.8 mA g^{-1}, a discharge capacity of 210 mA h g^{-1} was recovered, and then decreased gradually to a stable value of 203 mA h g^{-1} in the following cycles. This value is a little higher than the initial discharge capacity, which could originate from the homogeneous and ultrafine nano-LiF/Fe/G activated by cycling.

For comparison, the electrochemical performance of traditional microsized LiF/Fe/G material was also examined as shown in Figure 4. Figure 4a shows the morphology of the micro-LiF/Fe/G hybrid material, which reveals that micro-LiF and Fe/G cannot be homogeneously mixed. Figure 4b shows that charge and discharge capacities of the first cycle at 20.8 mA g^{-1} are 236 and 86 mA h g^{-1}, respectively, with a Coulombic efficiency of 36.4%. The reversible capacity is less than 50% of the nano counterpart. Furthermore, from the 50th to the 90th cycle, the capacity gradually increases from ∼70 to 115 mA h g^{-1}, which is caused by the pulverization of large micro-LiF particles into ultrafine LiF nanoparticles. It is well-known that the particle size has profound effect on the electrochemical activity of fluoride electrodes.[18] As shown in Figure S4 in the Supporting Information, the TEM image of the cycled micro-LiF/Fe/G hybrid material confirms that there are large amount of ultrafine nanoparticles (5−20 nm) that are highly dispersed in the graphene matrix, an indication of intensive pulverization of the large particles after long cycling. Very few large cubic shape particles that could be ascribed to the residual LiF can be found. The voltage profiles also demonstrate that after 50 cycles the plateau of discharge between 3.5 and 2.5 V becomes obvious (Figure 4c), clearly indicating that it is much harder to be activated for the micro-LiF/Fe/G samples. Figure 4d shows the rate capability of micro-LiF/Fe/G, which is substantially inferior to its nano compartment due to the large size of LiF particles and nonuniform mixing. Therefore, after downsizing LiF/Fe and incorporating them with graphene by ball-milling, the electrochemical performance of LiF/Fe/G can be considerably enhanced.

Graphene layers play an important role in imporving the electrochemical performance of the LiF/Fe/G nanocomposite. They not only serve as protective spacers to prevent the agglomeration of the Fe nanoparticles during the electrochemical procedure, but also act as conducting network to facilitate electron transport during electrochemical reaction. In contrast, acetylene carbon black is hard to form cross-linked network and to function as a spacer. To prove this point, nano-LiF/Fe/Carbon-black was also fabricated with the same procedure. SEM image shows that after reduction at 550 °C

dx.doi.org/10.1021/am302558w | ACS Appl. Mater. Interfaces 2013, 5, 892−897

some large particles with spherical shape appeared, which could be ascribed to the fusion of nano-Fe particles (Figure 5a). For

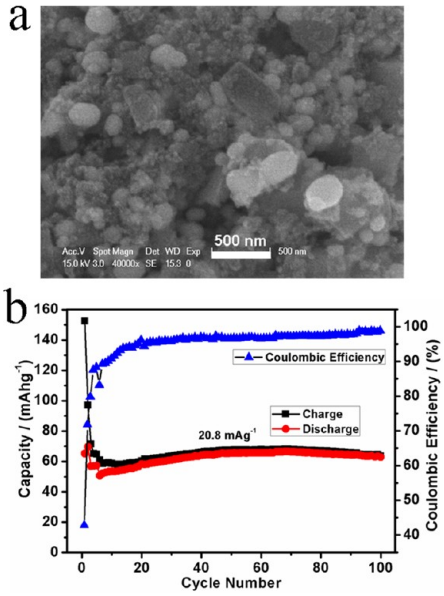

Figure 5. (a) SEM image and (b) cycling performance of LiF/Fe/carbon-black nanocomposite produced from reduction of nano-LiF/Fe_3O_4/carbon-black.

easy distinction, the morphology of carbon black was shown in Figure S5 in the Supporting Information. Electrochemical measurement shows that a very low reversible capacity of about 65 mA h g^{-1} at the current density of 20.8 mA g^{-1} was obtained, (Figure 5b) demonstrating inferior electrochemical perfomance with respect to nano-LiF/Fe/G.

To confirm the formation of FeF_x after fully charged, we disassembled the cycled batteries and investigated the cycled nano-LiF/Fe/G by ex situ XRD and TEM. Figure 6a shows the ex situ XRD patterns of the cycled nano-LiF/Fe/G. At the fully discharged state (I), only peakes related to Fe and LiF were detected. At the fully charged state (II), two evident peaks appeared at 35.7 and 62.9°, which could be indexed to cubic and tetragonal FeF_2, respectively, while a tiny peak located at 22.7° could be ascribed to the formation of FeF_3. This clearly indicates the formation of FeF_x in the charge process. The calculation of Li−Fe−F system by Doe et al., also revealed the coexistense of rutile FeF_2 and the defect trirutile FeF_3 at this state.[12] Furthermore, the Fe peak at 44.7° adjacent to LiF peak at 45° disappeared at the fully charged stage, an indication of the reaction of Fe with LiF to form FeF_x. It is also observed that the full width at half-maximum (fwhm) of peaks of LiF broadens compared to those in Figure 1d before cycling, further indicating that the LiF particles decreased to ultrafine nanoparticles upon cycling. Figure 6b shows the panoramic TEM image of nano-LiF/Fe/G after 50 cycles at the fully charged state. There are many uniform particles with a size of less than 20 nm, revealing that the cycled active material was pulverized into fine nanoparticles. The SAED (inset of Figure 6b), shows clearly identified concentric rings, indicating good crystallinity of the cycled powders. The high-magnification TEM image (Figure 6c) further reveals that even after 50 cycles the fine nanoparticles are still closely interconnected by the graphene, facilitating excellent and stable electron transport. It is reasonable to conclude that the incorporation of graphene with LiF and Fe is beneficial for the improvement of electronic conductivity. The HRTEM images (Figure 6 d&e), present more detailed structure of the cycled powders. The *d*-spacing of 0.203 nm agrees well with that of (200) plane of LiF (JCPDS No.45−1460) in Figure 6d, whereas the lattice fringes with spacings of 0.143 and 0.252 nm correspond to the planes of (200) and (222) of FeF_2 (JCPDS No.33−0649), respectively, in Figure 6e. It suggests that domains of LiF and FeF_2 coexist in the cycled active material, which is consistent with the ex situ

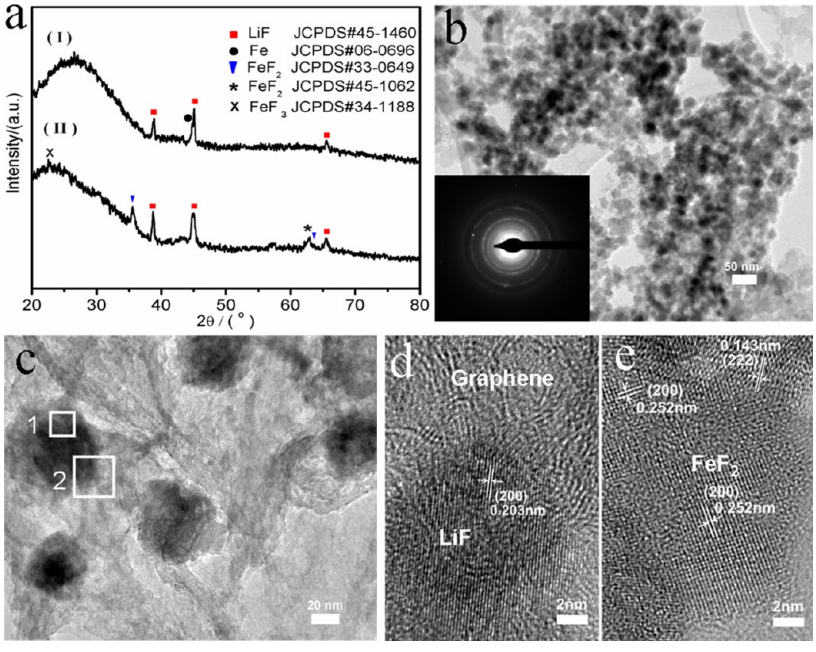

Figure 6. (a) Ex situ XRD patterns of the nano-LiF/Fe/G after fully discharged (I) and charged (II); (b) overview TEM image and (c) high-magnification TEM image of the nano-LiF/Fe/G after cycling; (d, e) HRTEM images of the marked areas 1 and 2 in c, respectively; inset of b shows the SAED of nano-LiF/Fe/G after cycling.

XRD pattern of curve (II) and the result reported in the literature.[22,24]

4. CONCLUSIONS

In summary, homogeneous LiF/Fe/G nanocomposites with stable cyclability and superior rate capability have been successfully fabricated by a two-step method, which not only avoids the use of highly corrosive reagents and expensive precursors but also fully takes advantage of the excellent electronic conductivity of graphene. The capacity remains to be higher than 150 mA h g^{-1} after 180 cylces, indicating high reversible capacity and stable cyclability. The comparison of electrochemical performance with micro-LiF/Fe/G and LiF/Fe/Carbon-black proves that graphene plays an important role not only in preventing the growth of Fe nanoparticles during reduction process but also in improving the electronic conductivity during charge/discharge. The ex situ XRD and HRTEM investigations on the LiF/Fe/G nanocomposites after cycling confirm the formation of FeF_x and the coexistence of LiF and FeF_x at the fully charged state. We believe that this novel kind of uniform nanocomposite of LiF/Fe/Graphene with nano-LiF and ultrafine Fe homogeneously dispersed on graphene sheets can be promising cathode materials for next-generation lithium ion batteries.

■ ASSOCIATED CONTENT

Ⓢ Supporting Information

XRD pattern of Fe_3O_4/G nanocomposites, TGA curve of Fe_3O_4/G nanocomposites in air and XRD pattern of the residue after TGA experiment, SEM image of micro-LiF, and TEM image of cycled micro-LiF/Fe/G hybrid material. This material is available free of charge via the Internet at http://pubs.acs.org.

■ AUTHOR INFORMATION

Corresponding Author

*E-mail: luzg@sustc.edu.cn (L.Z.G.); appchung@cityu.edu.hk (C.Y.C.). Fax: +852 3442 0538. Tel:+852 3442 7835.

Notes

The authors declare no competing financial interest.

■ ACKNOWLEDGMENTS

This work is supported by a GRF grant from the Research Grants Council of the Hong Kong S.A.R., China (Project CityU 100510). Z.G.L. acknowledges the support from the National Natural Science Foundation of China (21001117).

■ REFERENCES

(1) Goodenough, J. B.; Kim, Y. *J. Power Sources* **2011**, *196*, 6688−6694.
(2) Fergus, J. W. *J. Power Sources* **2010**, *195*, 939−954.
(3) Wang, Y. G.; Li, H. Q.; He, P.; Hosono, E.; Zhou, H. S. *Nanoscale* **2010**, *2*, 1294−1305.
(4) Chung, S. Y.; Bloking, J. T; Chiang, Y. M. *Nat. Mater.* **2002**, *1*, 123−128.
(5) Amatucci, G. G.; Pereira, N. *J. Fluorine Chem.* **2007**, *128*, 243−262.
(6) Xi, L. J.; Wang, H. E.; Lu, Z. G.; Yang, S. L.; Ma, R. G.; Deng, J. Q.; Chung, C. Y. *J. Power Sources* **2012**, *198*, 251−257.
(7) Lu, Z. G.; Cheng, H.; Lo, M. F.; Chung, C. Y. *Adv. Funct. Mater.* **2007**, *17*, 3885−3896.
(8) Zhu, J.; Zhu, T.; Zhou, X.; Zhang, Y.; Lou, X. W.; Chen, X.; Zhang, H.; Hng, H. H.; Yan, Q. *Nanoscale* **2011**, *3*, 1084−1089.
(9) Li, C. L.; Gu, L.; Tsukimoto, S.; van Aken, P. A.; Maier, J. *Adv. Mater.* **2010**, *22*, 3650−3654.
(10) Wang, F.; Robert, R.; Chernova, N. A.; Pereira, N.; Omenya, F.; Badway, F.; Hua, X.; Ruotolo, M.; Zhang, R.; Wu, L.; Volkov, V.; Su, D.; Key, B.; Whittingham, M. S.; Grey, C. P.; Amatucci, G. G.; Zhu, Y.; Graetz, J. *J. Am. Chem. Soc.* **2011**, *133*, 18828−18836.
(11) Badway, F.; Cosandey, F.; Pereira, N.; Amatucci, G. G. *J. Electrochem. Soc.* **2003**, *150*, A1318−A1327.
(12) Doe, R. E.; Persson, K. A.; Meng, Y. S.; Ceder, G. *Chem. Mater.* **2008**, *20*, 5274−5283.
(13) Zhou, M. J.; Zhao, L. W.; Doi, T.; Okada, S.; Yamaki, J. *J. Power Sources* **2010**, *195*, 4952−4956.
(14) Badway, F.; Pereira, N.; Cosandey, F.; Amatucci, G. G. *J. Electrochem. Soc.* **2003**, *150*, A1209−A1218.
(15) Kim, S. W.; Seo, D. H.; Gwon, H.; Kim, J.; Kang, K. *Adv. Mater.* **2010**, *22*, 5260−5264.
(16) Li, C. L.; Gu, L.; Tong, J.; Maier, J. *ACS Nano* **2011**, *5*, 2930−2938.
(17) Liu, L.; Zhou, M.; Yi, L.; Guo, H.; Tan, J.; Shu, H.; Yang, X.; Yang, Z.; Wang, X. J. *Mater. Chem.* **2012**, *22*, 17539−17550.
(18) Wu, W.; Wang, X.; Wang, X.; Yang, S.; Liu, X.; Chen, Q. *Mater. Lett.* **2009**, *63*, 1788−1790.
(19) Wu, W.; Wang, Y.; Wang, X.; Chen, Q.; Wang, X.; Yang, S.; Liu, X.; Guo, J.; Yang, Z. *J. Alloys Compd.* **2009**, *486*, 93−96.
(20) Li, H.; Richter, G.; Maier, J. *Adv. Mater.* **2003**, *15*, 736−739.
(21) Yu, X. Q.; Sun, J. P.; Tang, K.; Li, H.; Huang, X. J.; Dupont, L.; Maier, J. *Phys. Chem. Chem. Phys.* **2009**, *11*, 9497−9503.
(22) Wall, C.; Prakash, R.; Kubel, C.; Hahn, H.; Fichtner, M. *J. Alloys Compd.* **2012**, *530*, 121−126.
(23) Amatucci, G. G.; Pereira, N.; Badway, F.; Sina, M.; Cosandey, F.; Ruotolo, M.; Cao, C. *J. Fluorine Chem.* **2011**, *132*, 1086−1094.
(24) Prakash, R.; Mishra, A. K.; Roth, A.; Kubel, C.; Scherer, T.; Ghafari, M.; Hahn, H.; Fichtner, M. *J. Mater. Chem.* **2010**, *20*, 1871−1876.
(25) Prakash, R.; Wall, C.; Mishra, A. K.; Kuebel, C.; Ghafari, M.; Hahn, H.; Fichtner, M. *J. Power Sources* **2011**, *196*, 5936−5944.
(26) Singh, V.; Joung, D.; Zhai, L.; Das, S.; Khondaker, S. I.; Seal, S. *Prog. Mater. Sci.* **2011**, *56*, 1178−1271.
(27) Wang, Z. L.; Xu, D.; Huang, Y.; Wu, Z.; Wang, L. M.; Zhang, X. B. *Chem. Commun.* **2012**, *48*, 976−978.
(28) Song, H.; Zhang, L.; He, C.; Qu, Y.; Tian, Y.; Lv, Y. *J. Mater. Chem.* **2011**, *21*, 5972−5977.
(29) Kang, K. S.; Meng, Y. S.; Breger, J.; Grey, C. P.; Ceder, G. *Science* **2006**, *311*, 977−980.
(30) Li, X. Y.; Huang, X. L.; Liu, D. P.; Wang, X.; Song, S. Y.; Zhou, L.; Zhang, H. J. *J. Phys. Chem. C* **2011**, *115*, 21567−21573.
(31) Chen, D. Y.; Ji, G.; Ma, Y.; Lee, J. Y.; Lu, J. M. *ACS Appl. Mater. Inter.* **2011**, *3*, 3078−3083.
(32) Beaulieu, L. Y.; Larcher, D.; Dunlap, R. A.; Dahn, J. R. *J. Electrochem. Soc.* **2000**, *147*, 3206−3212.
(33) Zhang, K. J.; Han, P. X.; Gu, L.; Zhang, L. X.; Liu, Z. H; Kong, Q. S.; Zhang, C. J.; Dong, S. M.; Zhang, Z. Y.; Yao, J. H; Xu, H. X.; Cui, G. L.; Chen, L. Q. *ACS Appl. Mater. Inter.* **2012**, *4*, 658−664.
(34) Lin, Y. M.; Abel, P. R.; Heller, A.; Mullins, C. B. *J. Phys. Chem. Lett.* **2011**, *2*, 2885−2891.